https://doi.org/10.1595/205651318X696837 *Johnson Matthey Technol. Rev.*, 2018, **62**, (4), 364–382

JOHNSON MATTHEY
TECHNOLOGY REVIEW

www.technology.matthey.com

Optimisation of a Jewellery Platinum Alloy for Precision Casting: Evaluation of Mechanical, Microstructural and Optical Properties

Two new platinum alloys proposed for jewellery use

Tanja Trosch
University Bayreuth, Metals and Alloys, Ludwig-Thoma-Str. 36b, 95447 Bayreuth, Germany

Fanny Lalire
VV, Branch of Richemont International SA, Rue St-Georges 7, 2800 Delémont, Switzerland

Stéphane Pommier
VV, Branch of Richemont International SA, Rue St-Georges 7, 2800 Delémont, Switzerland

Rainer Völkl
University Bayreuth, Metals and Alloys, Ludwig-Thoma-Str. 36b, 95447 Bayreuth, Germany

Uwe Glatzel*
University Bayreuth, Metals and Alloys, Ludwig-Thoma-Str. 36b, 95447 Bayreuth, Germany

***Email:** uwe.glatzel@uni-bayreuth.de

An optimal platinum alloy for precision casting was developed by taking 25 possible alloying elements into consideration. In order to rank these elements an equation was designed. The ranking allowed five promising alloy compositions to be identified. From these five alloys arc melted buttons were produced and tested for homogeneity and hardness to ensure their suitability as jewellery alloys. A pyrometer was used to measure solidus temperatures. In a second iteration, the five alloys were further improved and the most promising alloys were cast and compared to a commonly used jewellery alloy: platinum-copper-gallium (PtCuGa). The comparison was based on the melting interval and on microstructural investigations, carried out by scanning electron and optical microscopy, while mechanical properties were determined by tensile testing. Additionally, optical properties such as reflectivity and colour were investigated. After the second iteration two very promising compositions were identified: PtCuFeMnCr and PtCuFePdVY.

1. Introduction

In the field of precious metals, platinum stands out due not only to its high monetary value, but also to its excellent properties with regard to oxidation and biocompatibility. This makes jewellery the world's second largest application for platinum after the autocatalyst market (1). However, in addition to all the useful properties of platinum, there are some characteristics which challenge jewellery manufacturers. Pure platinum is very soft and therefore not suitable for everyday use. The addition of alloying elements, which promote better mechanical and microstructural properties, are strictly limited to less than 5 wt% since the alloy must have a guaranteed minimum platinum content of 95 wt% to be considered as an internationally recognised platinum jewellery alloy (2).

A common production method for platinum jewellery is the precision casting process, in which a preformed wax model is attached to a sprue together with other wax models to form a wax

tree. The wax tree is then formed in investment material and burned in a furnace to obtain a negative form, which is filled with the molten metal (3, 4). Casting platinum is challenging due to its high melting point of 1769°C. The high casting temperatures make precision casting of filigree parts more difficult and the addition of elements to reduce the liquidus temperature is beneficial. A low liquidus temperature leaves enough room for overheating the melt, which could promote form filling, prevents possible damage of the crucible and reduces the reaction with the investment material.

Figure 1 shows the requirements for developing a new casting alloy for jewellery used in this work. The new alloy should meet these requirements and should be equal to or exceed the benchmark alloy PtCuGa with 1.8 wt% copper and 2.9 wt% gallium. All these requirements must be met by the addition of only 5 wt% alloying elements.

In a first step, the possible alloying elements were selected by exclusion of unsuitable elements. All radioactive, toxic and allergenic elements were excluded to produce a safe and health compatible alloy. Also, critical raw materials such as rare earth elements with potential supply risks, or elements which cause difficulties or a health hazard during the manufacturing process were eliminated. This led to 25 remaining elements (highlighted in green in **Figure 2**).

2. Materials and Methods

2.1 Ranking of Elements and their Concentrations

Based on literature research the influences on platinum of the shortlisted 25 elements were combined in a single equation to arrange these

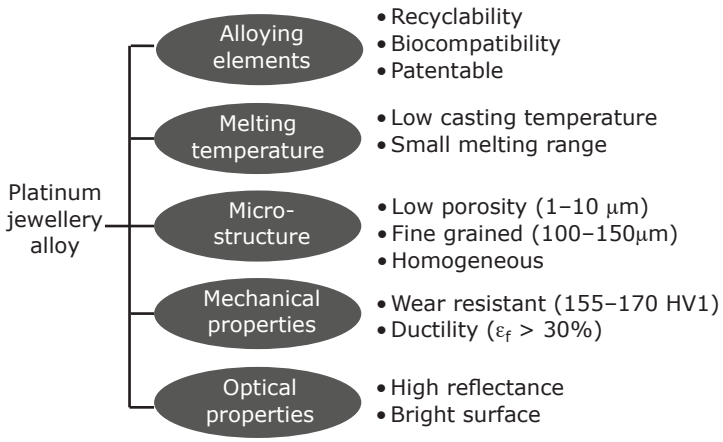

Fig. 1. Requirements for an optimum casting alloy for platinum jewellery

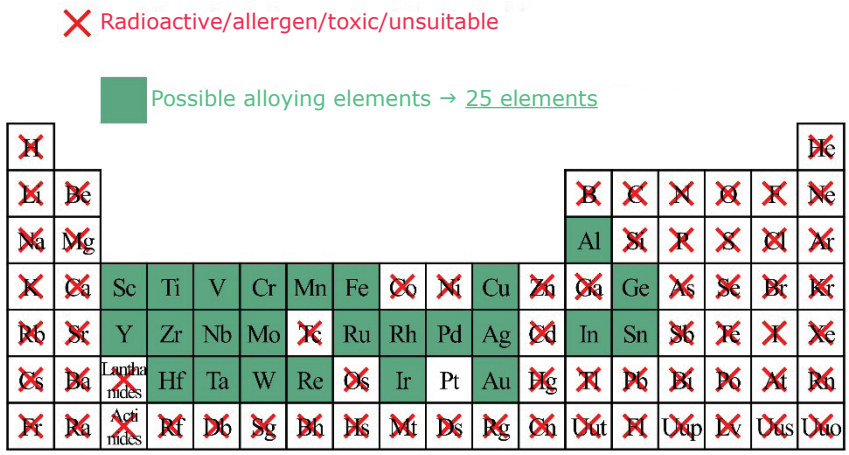

Fig. 2. The 25 remaining alloying elements highlighted in green after exclusion of radioactive, allergenic, toxic and other unsuitable elements

elements according to their suitability. The suitability index of an element is the combination of four characteristics:

- maximum solubility in platinum ($c_{max.sol.}$)
- hardness index (hi)
- melting interval index (mii)
- liquidus temperature change index ($T_l$ci).

We define the four characteristics of an element combined equally by linear superposition in Equation (i):

$$\text{Suitability index} = c_{max.sol.} + \text{hi} + \text{mii} + T_l\text{ci} \quad \text{(i)}$$

Each individual term can take up a value in the range of 0–100 as dimensionless scalars. Therefore Equation (i) has a minimum output value of zero and a maximum of 400. The higher the value, the more suitable the element for a platinum jewellery alloy, according to the requirements of **Figure 1**. The individual terms of Equation (i) are explained in detail below.

2.1.1 Concentration of Maximum Solubility

In the new alloy, the elements should be distributed as homogeneously as possible and form a single-phase solid solution face-centred-cubic (fcc) alloy. For this, the solubility of the respective element in platinum must not be exceeded. However, by casting the alloys, segregation may occur in which the elemental concentration exceeds the nominal concentration and thereby exceeds the maximum solubility of the element. This term of the equation promotes elements with higher solubility, which are less likely to form intermetallic phases.

Figure 3 shows the solubility maximum of each element in platinum in units of wt% obtained from the respective binary phase diagrams (5). It reaches values from 0.2 wt% (Y) to 100 wt% (Au). The right side shows the normalised scale with the dimensionless solubility value $c_{max.sol.}$ used in Equation (i). The elements gold, palladium, rhodium, copper and iridium reach the maximum $c_{max.sol.}$ value of 100 and are thus best suited to form a solid solution, while yttrium is only soluble to a maximum of 0.2 wt% and therefore receives the lowest value for $c_{max.sol.}$ = 0. The $c_{max.sol.}$ of manganese is 15, since manganese can be dissolved in platinum up to 15 wt% (5).

2.1.2 Hardness Index

All alloying elements have a hardness increasing influence on pure platinum with an initial Vickers hardness of ~40 HV1 (6). The hardness range which provides the ideal compromise between workability and wear resistance is set by many years of experience to 155–170 HV1. We define the hi by Equation (ii):

$$\text{hi} = 100 - 1/6.53 \times \sqrt{(323 - \Delta\text{HV1/wt\%} \times 5\ \text{wt\%})^2} \quad \text{(ii)}$$

The hi is given as a dimensionless value in a range of 0–100 and represents the distance to the ideal hardness range that results from 5 wt% addition of the respective element. The addition of 5 wt% yttrium would result in a theoretical hardness of 815 HV1, which leads to the largest distance of 653 HV1 from the ideal hardness mean value of 163 HV1. Therefore, the lowest value of hi = 0.

Figure 4 shows the influence of the hardness of each element. The blue line represents the increase in hardness due to a 1 wt% addition of the respective element and the hi, represented by the green line, indicates the extent to which the elements contribute to the achievement of the optimum hardness range of 155–170 HV1. The hi serves to estimate the quantity of an element

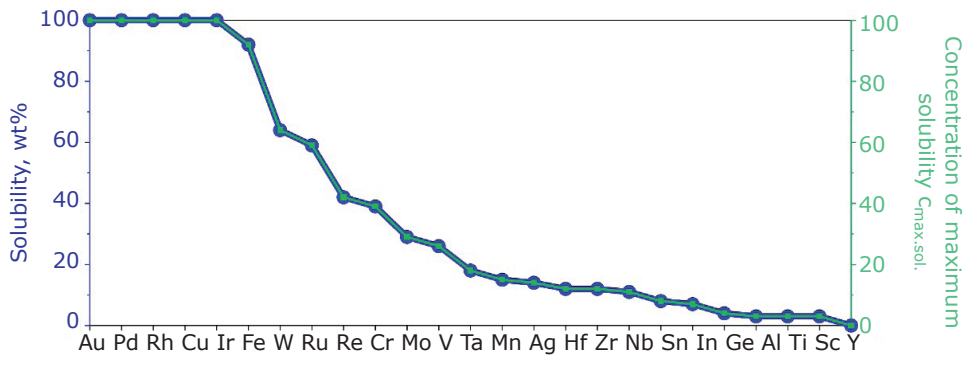

Fig. 3. Solubility of elements in platinum (5). Elements are sorted by decreasing $c_{max.sol.}$

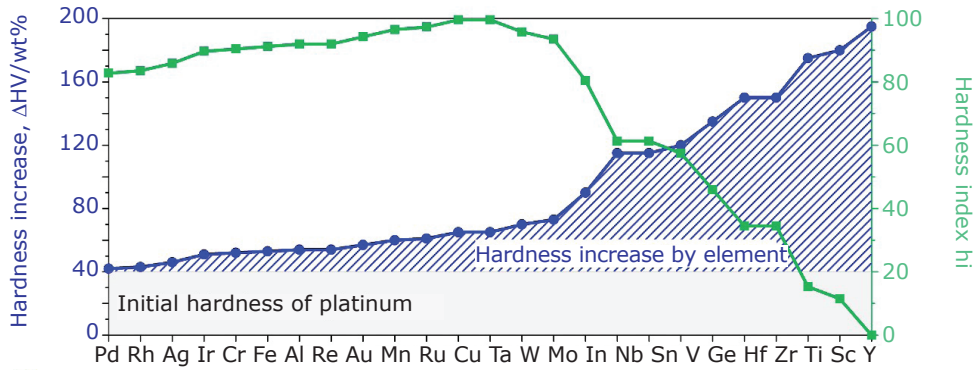

Fig. 4. Influence of the alloying elements on the hardness of platinum (6–13). Elements are sorted by increasing hardness, while hi (Equation (ii)) has its maximum in the centre

which should be added in order to reach the desired hardness range. As another example 1 wt% of the element manganese increases the hardness by 20 HV1. To increase the initial platinum hardness of 40 HV1 to the desired level of 155–170 HV1 a manganese addition of 5.75–6.5 wt% is required. This results in hi = 97 for manganese.

The elements titanium, scandium and yttrium contribute most to the hardening of platinum (135 HV1, 140 HV1 and 155 HV1 per wt%), while the hardness is only slightly increased by palladium, rhodium and silver (2 HV1, 3 HV1 and 6 HV1 per wt%).

In **Figure 4**, the elements with the optimal influence on hardness are arranged in the middle, shown by the maximum hi close to 100. Large amounts of these elements can be added and the desired hardness range will still be reached. When elements are added from the left side of the maximum hi, the alloy remains too soft. On the other hand, when elements are added from the right side the hardness increase can quickly become too high even if only small quantities are added, therefore hi takes very low values.

2.1.3 Melting Interval Index

This term represents the negative effect of a large melting interval, the difference between liquidus temperature T_l and solidus temperature T_s. A narrow melting interval is advantageous for less segregation and smaller grains. The melting interval of each platinum based binary alloy is determined at the concentration of 5 wt% of the respective element as shown in the example of a detailed part of the silver-platinum binary diagram in **Figure 5**. If, for example, a platinum alloy with 5 wt% silver is considered, the melting interval is 85°C.

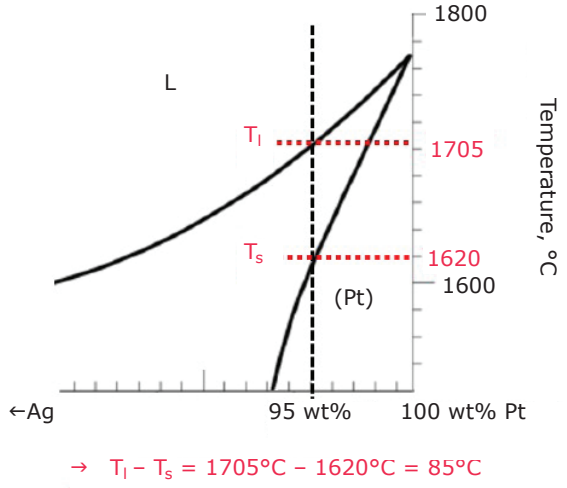

Fig. 5. The determination of the melting interval at 95 wt% platinum in the binary phase diagram silver-platinum (3). Detail at the platinum rich side and temperature range of 1500–1800°C is shown

In **Figure 6** the melting intervals for the platinum based binary alloys at, in some cases hypothetical, 5 wt% are shown. For elements with low solubility, the initial slope was extrapolated to 5 wt%. The value of the mii is normalised with respect to the maximum occurring melting interval of 500°C, which is the melting interval of platinum with 5 wt% germanium. We define the mii by Equation (iii):

$$mii = 100 - (T_l - T_s)/5°C \quad \text{(iii)}$$

Thereby mii turns out to be dimensionless in the range of 0–100, as seen on the right axis in **Figure 6**. The value of mii for copper is 100, since the melting interval of copper is close to 0°C. The mii of germanium is zero since its hypothetical melting range at 5 wt% germanium content is 500°C. Manganese as an example

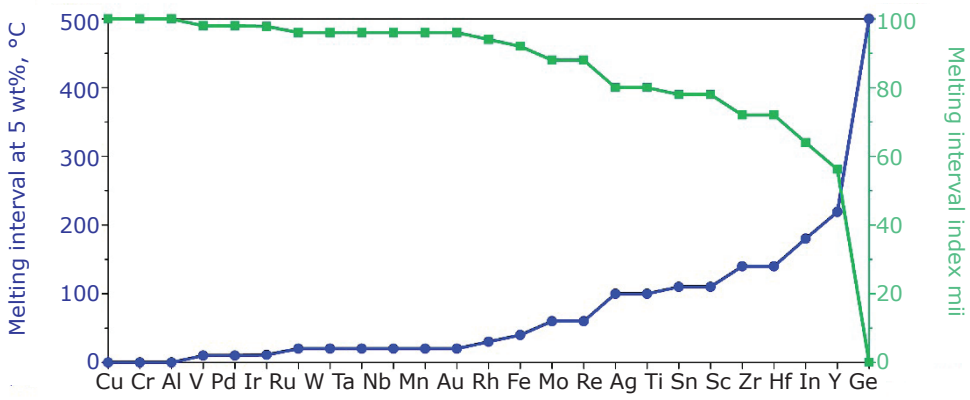

Fig. 6. Melting interval of the platinum based binary alloys at a concentration of 5 wt%, taken from the binary phase diagrams (3). Elements are sorted by decreasing mii (Equation (iii)), in some cases a hypothetical melting interval is used

creates a melting interval of 20°C, which results in a mii = 96.

2.1.4 Liquidus Temperature Change Index

The precision casting in this work was carried out at 200°C overheat above the liquidus temperature T_l in order to allow the casting of very fine filigree parts. To prevent possible damage to the crucible and reduce reaction with the investment material the liquidus temperature of the new alloys should be as low as possible. The reduction or increase of the liquidus temperature T_l by alloying an element at 5 wt% is represented by the slope which is described as ΔT_l/5 wt% with ΔT_l in °C, as shown in **Figure 7**. The slope in **Figure 7** is obtained from the binary phase diagrams and had to be extrapolated for some elements to 5 wt%.

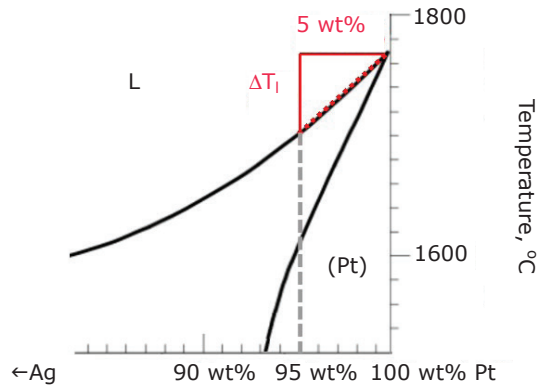

Fig. 7. Influence on the liquidus temperature by the addition of silver to platinum (3). Detail at the platinum rich side and temperature range of 1500–1800°C is shown

The slope in **Figure 7** describes the alteration of the liquidus temperature by addition of 5 wt% of alloying element. A positive slope results in reduction of the liquidus temperature as seen in the example of the silver-platinum binary system and a negative slope results in an increase of the liquidus temperature, if platinum is on the right side of the binary phase diagram.

In **Figure 8** the liquidus temperature lowering elements (negative slope of ΔT_l/5 wt%) are shown on the left with the normalised values of $T_l$ci shown on the right side. We define the influence of the $T_l$ci by Equation (iv):

$$T_l ci = - 0.855\ (wt\%/°C)\ (\Delta T_l/5wt\%) + 34.2 \quad (iv)$$

Aluminium reduces the liquidus temperature very strongly, with a reduction of –77°C per 5 wt%, leading to $T_l$ci = 100. Scandium strongly increases the liquidus temperature of platinum by +40°C per 5 wt% addition, therefore $T_l$ci = 0. Manganese reduces the liquidus temperature by –23°C, leading to $T_l$ci = 54.

Table I lists the elements in order of decreasing suitability index, from Equation (i). An alloying element with a high suitability index value, like copper (suitability index = 340), gold (suitability index = 330) and palladium (suitability index = 315), has a positive influence according to Equation (i) and can be added in large amounts, whereas scandium (suitability index = 93), yttrium (suitability index = 118) and titanium (suitability index = 125) should be added very carefully.

Additionally, each element must be examined more closely with respect to other influences, which might overrule the suitability index obtained

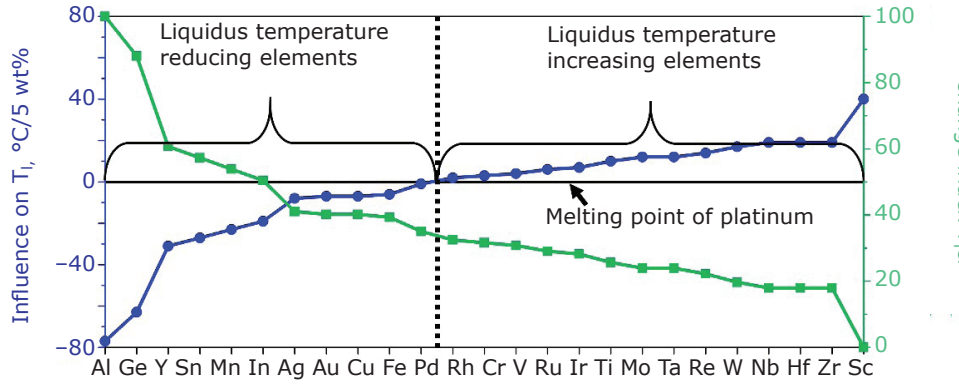

Fig. 8. Influence on T_l by 5 wt% addition of the respective alloying element (3). Elements sorted by decreasing liquidus temperature change index $T_l$ci (Equation (iv))

Table I Suitability of Elements With Additional Key Properties Mentioned in the Last Column

Element	$c_{max.sol.}$	hi	mii	$T_l$ci	Suitability index	Property (7, 8, 11, 14–20)
Cu[a, b]	100	100	100	40	340	Good form filling
Au[a]	100	94	96	40	330	Expensive
Pd[a, b]	100	83	98	35	316	Similar to Pt
Ir[a]	100	89	98	28	315	Grain finer
Fe[a, b]	92	91	92	39	314	Low cost
Rh[a]	100	84	94	32	310	Grain finer
Al[a]	3	92	100	100	295	Strong precipitate former
Ru	59	97	96	29	281	Grain finer
W[b]	64	96	96	20	276	High strength
Mn[a, b]	15	97	96	54	262	High vapour pressure
Cr[a, b]	39	90	100	32	261	Corrosion resistance
Re	42	92	88	22	244	Good patentable
Ta	18	100	96	24	238	Good patentable
Mo	29	93	88	24	234	Good patentable
Ag	14	86	80	41	221	Strong precipitate former
V[a, b]	26	57	98	31	212	Grain finer
Sn	8	61	78	57	204	Good patentable
In	7	80	64	50	201	Strong precipitate former
Nb	11	61	96	18	186	High strength
Ge[b]	4	46	0	88	138	Good patentable
Zr	12	34	72	18	136	Grain finer
Hf	12	34	72	18	136	Good patentable
Ti	3	15	80	26	124	High temperature strength
Y[b]	0	0	56	61	117	Grain finer
Sc	3	11	78	0	92	Good patentable

[a] Element used in the first iteration

[b] Element used in the second iteration

by Equation (i). For example some elements have an influence on grain refinement (rhodium, ruthenium), which consequently is important for mechanical and optical properties (19), or corrosion resistance (chromium). Therefore an extended literature search was done including platinum jewellery alloys, industrially used platinum alloys and platinum based superalloys (15, 16, 20–23). All the information combined with the suitability index led to the selection of elements with different

concentrations in the alloy compositions which were investigated in this work and are listed in **Table II** for the first iteration and **Table III** for the second iteration.

2.2 Sample Production by Arc Melting and Precision Casting

All alloys were prepared using an argon arc melting furnace (Edmund Bühler GmbH, Germany) with a chilled copper plate and a tungsten electrode under argon atmosphere at a pressure of 5×10^4 Pa, while T_s was determined by a quotient pyrometer attached to the arc melting furnace. Five different alloys in the first iteration referred to as A1, B1, C1, D1, E1 and five different alloys in the second iteration referred to as A2, B2, C2, D2, E2 with minimum 95 wt% platinum and maximum 5 wt% of varying alloying elements were arc melted. All raw materials had a purity of at least 99.9%. The sample size was 10 g and it was melted and subsequently remelted four times, which caused a mass loss for elements with a low vapour pressure like manganese. The relative mass loss was always below 1% after arc melting.

After investigating the microstructure, hardness and melting interval for the 10 g buttons of all ten alloys the promising alloy compositions were prepared in 50 g samples by arc melting and subsequently processed by precision casting.

Due to the fact that the alloys were primarily designed to be processed by gravity casting, casting tests were performed with the tilt casting machine MC 20 V (Indutherm GmbH, Germany) (**Figure 9**). The assumption was that as soon as the alloys show sufficient form filling abilities after gravity casting, good form filling will also apply to centrifugal casting. Next to the determination of form filling ability, parts were designed for the evaluation of mechanical, microstructural and

Table II Composition of the Five Alloys of the First Iteration. Security Balance is Comprised Between 0.1 wt% and 0.5 wt% to Ensure a Minimum Platinum Content of 95 wt% in the Cast Part

Alloy		Pt	Cu	Au	Al	Fe	Ir	Pd	Rh	Mn	Cr	V
A1	wt%	95.0	0.5	–	1.5	0.3	–	–	–	2.1	0.3	–
	at%	81.5	1.3	–	9.3	0.9	–	–	–	6.1	0.9	–
B1	wt%	95.0	0.3	0.4	–	–	–	2.0	–	–	–	2.0
	at%	88.3	0.8	0.4	–	–	–	3.4	–	–	–	7.1
C1	wt%	95.0	–	–	–	–	1.9	1.1	1.1	0.6	–	–
	at%	92.1	–	–	–	–	1.9	1.9	2.0	2.1	–	–
D1	wt%	95.0	0.7	2.2	–	–	–	1.2	–	0.6	–	–
	at%	91.6	2.1	2.1	–	–	–	2.1	–	2.1	–	–
E1	wt%	95.0	–	–	–	–	0.3	1.0	0.3	3.1	–	–
	at%	87.4	–	–	–	–	0.3	1.7	0.5	10.1	–	–

Table III Composition of the Five Alloys of the Second Iteration. Security Balance is Comprised Between 0.1 wt% and 0.5 wt% to Ensure a Minimum Platinum Content of 95 wt% in the Cast Part

Alloy		Pt	Cu	Fe	Pd	W	Mn	Cr	V	Ge	Y
A2	wt%	95.0	1.3	1.2	–	–	1.1	1.1	–	–	–
	at%	85.5	3.6	3.7	–	–	3.5	3.7	–	–	–
B2	wt%	95.0	0.3	1.0	1.5	–	–	–	1.8	–	0.1
	at%	87.0	0.8	3.2	2.5	–	–	–	6.3	–	0.2
C2	wt%	95.0	–	1.0	1.1	1.0	0.6	–	–	1.0	–
	at%	89.3	–	3.3	1.9	1.0	2.0	–	–	2.5	–
D2	wt%	95.0	0.7	1.1	1.2	–	0.6	–	–	1.1	–
	at%	87.8	2.0	3.5	2.0	–	2.0	–	–	2.7	–
E2	wt%	95.0	–	0.3	1.0	–	3.0	–	–	0.3	0.1
	at%	86.8	–	0.9	1.7	–	9.7	–	–	0.7	0.2

optical properties of the alloys. To obtain all these test results with one test geometry the design of the model required particular preparation. The setup of the model is an important point, since the geometry of the main sprue, the angle and position of the single parts have a strong influence on the filling of the mould. Different platinum casting models were investigated and based on these results, a model was designed and 3D printed (Kudo 3D Inc, USA) with castable resin (Castable Blend, FunToDo, The Netherlands) to achieve consistent results (24–27). After successful trial casts with a good castable platinum alloy the final model was determined and is shown in **Figure 10**.

All parts are mounted at an angle of 60°. The two elongated square shaped parts with dimensions 28 × 4.5 × 3 mm^3 are attached to the sprue for evaluating mechanical and microstructural properties. Furthermore a grid for evaluating the form filling ability of the alloy is attached together with a platelet of diameter 20 mm and thickness 1.5 mm, which is used for optical property measurements.

The investment material used was Pro HT Platinum (Gold Star Powders, UK). It is a water based phosphate bonded powder, which was prepared in a vacuum mixing machine (Indutherm GmbH) with an exact water to powder ratio of 100:585 (28, 29). After stirring for 3 min under vacuum the mixture was poured over the model into a steel flask where it was left for at least 3 h for curing. For burnout, the mould was slowly heated up to 150°C where it was held for 1.5 h. During this period the castable resin started to soften. Subsequently the temperature was raised to the final mould temperature of 950°C during which time the resin burned free of residuals. After at least 1 h at casting temperature the flask and crucible were put into the casting machine (MC 20 V, Indutherm GmbH) and the casting was started immediately (**Figure 9**). The temperature inside the crucible

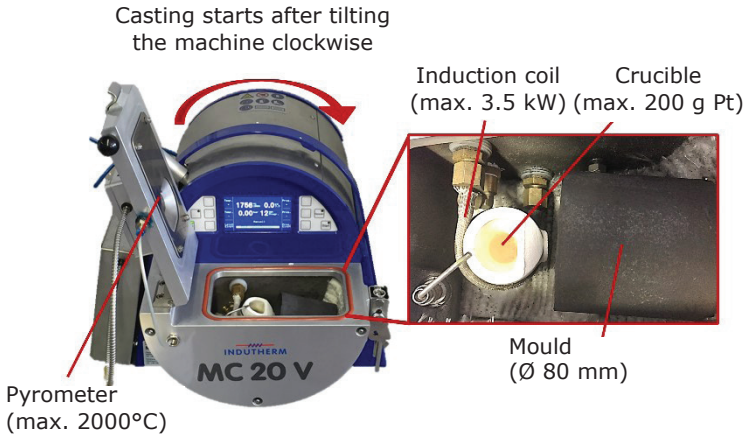

Fig. 9. Casting machine MC 20 V (Indutherm GmbH, Germany)

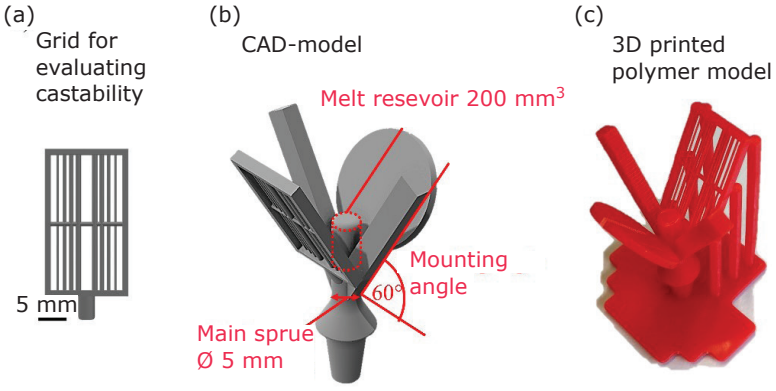

Fig. 10. (a) Grid for evaluation of the form filling, (b) CAD model and (c) 3D printed polymer model made of castable resin used for precision casting

was measured by a quotient pyrometer with a measurement range of 500–2000°C.

After the chamber was flushed twice with argon gas, the induction heating started under argon atmosphere at 1×10^4 Pa and the platinum reached the casting temperature of about 1700–1800°C after a heating time of around 2 min. The alloy was then cast into the mould with a temperature of 925–930°C. After tilting the crucible, the pressure in the chamber was raised to 3×10^5 Pa and the filled flask was left to cool for 3 min. After cooling, the flask was removed from the casting machine and left for 10 min before removing the investment by water quenching. The cast part was cleaned in an ultrasonic bath and the rest of the investment material was removed with a hand brush.

2.3 Microstructural Investigations

The microstructure was examined by optical and scanning electron microscopy (SEM) (1540 EsB Crossbeam, Zeiss, Germany) equipped with an energy dispersive X-ray spectroscopy (EDS) detector (Thermo Fisher Scientific, USA) and operating at 20 kV using the secondary electron signal for imaging. Specimens for microstructure analysis were ground, polished and subsequently run on a VibroMet™ (Buehler, USA) in a 0.6 µm diamond suspension with 2% HCl to obtain a deformation free etched surface. Porosity measurements were evaluated based on optical microscopic images with the analysis software Stream® Motion (OLYMPUS Corp, Japan). Grain size analysis was carried out with an electron back scattered detector (EBSD) (Sigma™ 300 VP Gemini®, Zeiss) equipped with a Hikari EBSD camera (EDAX Inc, USA). For measurements, a step size of 6 µm and a misorientation angle of 5° were chosen. Due to the deformation-free preparation of the sections a sufficient indexing rate, which is a measure of the accuracy in the determination of the EBSD patterns, of at least 90% was achieved. The data was evaluated with TEAM™ EBSD analysis in combination with the orientation imaging microscopy analysis (OIM Analysis™) system (EDAX Inc). The possible presence of intermetallic phases was checked with an X-ray diffraction (XRD) system (D8 Advance, Bruker, USA) equipped with a Cu anode and a Ge monochromator separating Cu-Kα_1 from Cu-Kα_2.

2.4 Mechanical Properties

Vickers microhardness tests with a load of 9.81 N (HV1) were carried out on the horizontally divided arc melted 10 g buttons. These were preliminary tests to eliminate alloys which differed greatly from the required hardness values. The hardness measurements were then repeated on the cast samples for verification. Tensile testing was carried out in air at room temperature. By wire electrical discharge machining (EDM) it was possible to cut out three tensile specimens per elongated square shaped part. **Figure 11** shows the geometry of the tensile specimen. The total length of the specimen was 17.6 mm cut out of the cast elongated square shaped part with a length of 28 mm, indicated by the blue rectangle.

For tensile testing the specimen was clamped in an upright position by form fitting grips, which were then fixed in the tensile testing device as shown in **Figure 12**. Strain was measured optically by a charge-coupled device (CCD) camera with blue backlight illumination which recorded the movement of the four ridges in the centre of the tensile specimen.

2.5 Optical Properties

Evaluation of the visual appearance of the alloy, colour and surface reflectance were carried out with specular component included, using a spectrometer (LAMBDA 950 Flex, PerkinElmer, Poland) with the standard daylight illuminant D65.

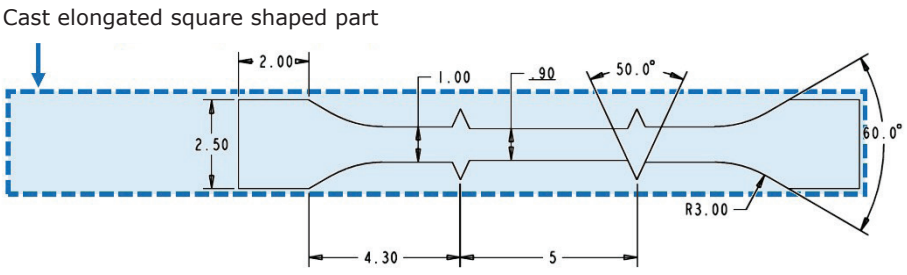

Fig. 11. Miniature tensile specimen cut out of the cast elongated square shaped parts by wire EDM

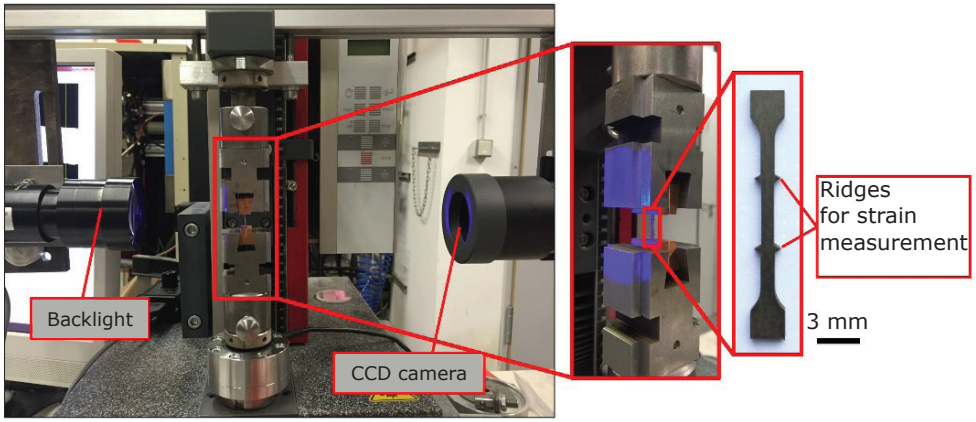

Fig. 12. Tensile testing device for miniature specimen based on a test setup (30, 31)

A Commission Internationale de l'Éclairage (CIE) standard observer angle of 2° was used. The measuring range of 380–780 nm was divided into intervals of 10 nm.

For colour measurements, the cast platelet was prepared according to the specifications of ISO 8654:2018. The colour was obtained by spectral reflectance measurements in accordance with CIE Publication 038-1977 (32). The obtained optical measurement data points are represented in the CIE colour system using the coordinates L*, a* and b* as shown in simplified form in **Figure 13**. L* represents the lightness, a* the red-green hue and b* the yellow-blue hue.

3. Results and Discussion

3.1 First Alloy Iteration

Based on the results of Equation (i), listed in **Table I**, and other important influences, the compositions of the first alloy iteration (A1–E1) were determined, see **Table II**. It was ensured that all alloys had a novel unique composition.

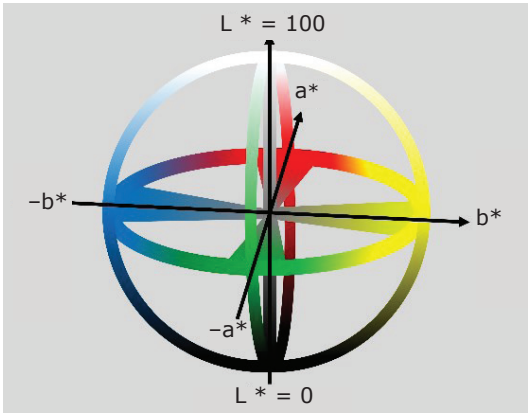

Fig. 13. The CIE colour space with the coordinates L*, a* and b*

- A1 contained 17.6 at% of liquidus temperature lowering elements (aluminium, manganese, copper and iron with $T_l ci \geq 40$) to promote good form filling and manganese and chromium for increased hardness
- B1 contained 7.1 at% vanadium for sufficient hardness. Copper, gold and palladium are not only liquidus temperature decreasing but also 100% soluble in platinum
- C1 contained palladium, manganese, iridium and rhodium in equal atomic distribution of 2 at% each. With palladium, iridium and rhodium being 100% soluble, a single-phase solid solution alloy with sufficient hardness was expected
- D1 contained the elements copper, palladium, manganese and gold, distributed in the same atomic ratio of 2.1 at% each. With manganese being the only non-100% soluble element, a single-phase microstructure was expected
- E1 was composed of the same elements as C1 with a higher amount of manganese to obtain higher hardness.

Before the precision casting of the alloys the preliminary results of the arc melted buttons concerning possible precipitates are shown in **Figure 14**.

The XRD analysis on the benchmark alloy PtCuGa showed peaks that match the $L1_2$ structure of the Pt_3Ga phase, on which the hardenability of the alloy is based. Due to interdendritic segregation of aluminium in alloy A1, as shown in **Figure 15**, the solubility limit of 3 wt% in the platinum solid solution was exceeded, which led to the formation of Pt_3Al.

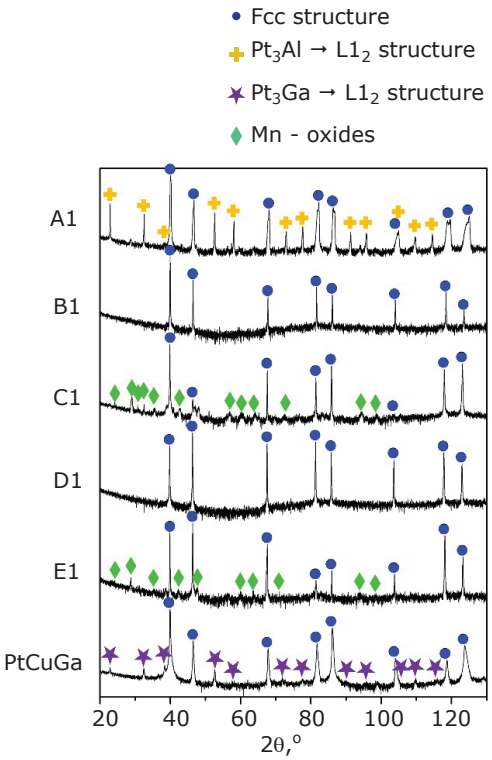

Fig. 14. XRD measurements of the five alloys of the first iteration processed by arc melting in comparison to the benchmark alloy Pt-1.8 wt% Cu-2.9 wt% Ga

The compositions of alloys C1 and E1 led to a reduction in oxidation resistance, since the XRD pattern shows peaks of manganese oxides. Concerning the microstructure of the alloys it turned out that only B1 and D1 show a single-phase microstructure.

Hardness and melting temperatures (pyrometer attached to arc melting furnace) were obtained by investigating the arc melted samples, see **Table IV**.

The solidus temperature of each alloy was determined by pyrometer during the arc melting process and revealed solidus temperatures for C1, D1 and E1 ranging from 1700–1800°C. This would lead to estimated liquidus temperatures of at least 1800–1900°C and therefore these alloys should be improved in a second alloy iteration to lower their melting interval, since it was one aim of the work to find a low melting platinum alloy similar to the melting interval of PtCuGa, where the reaction with the investment material and crucible damage are reduced. The solidus temperature of PtCuGa was found at 1320°C, followed by A1 at 1400°C and B1 at 1530°C.

Table IV Solidus Temperature and Hardness of the Five Alloys of the First Iteration Processed by Arc Melting in Comparison to the Benchmark Alloy Pt-1.8 wt% Cu-2.9 wt% Ga

Alloy	T_s, °C	Hardness[a] in HV1
PtCuGa	1320	225 ± 25
A1	1400	279 ± 30
B1	1530	164 ± 6
C1	1800	95 ± 3
D1	1700	109 ± 5
E1	1800	147 ± 6

[a] Each value was determined from an average of 20 measurements

The required hardness values of 155–170 HV1 were best met by alloy B1, followed by E1, of which the hardness was slightly below the required range. The hardness of PtCuGa at 225 HV1 is considered very hard and difficult to process, therefore alloy A1 is too hard for use as a jewellery alloy. This may be caused by the local formation of the Pt_3Al phase, which is indicated by the large scatter in hardness. Due to the low hardness of alloys C1 and D1 their wear resistance is insufficient.

These results lead to the conclusion that B1 meets the minimum requirements for a castable platinum

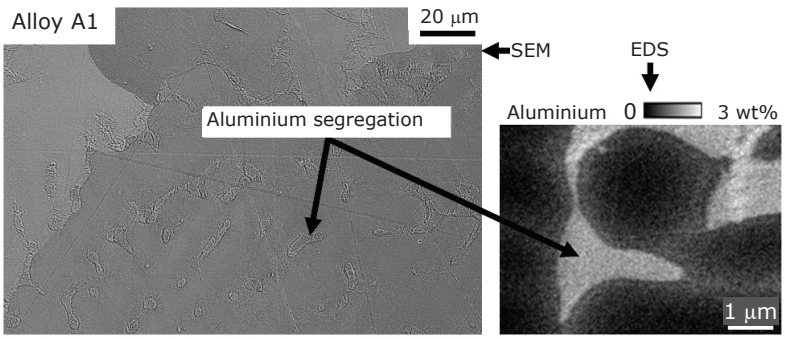

Fig. 15. Interdendritic aluminium segregations that lead to the formation of Pt_3Al

jewellery alloy, whereas the alloys A1, C1, D1 and E1 do not. This led to the development of a second alloy iteration, see **Table III**.

Aluminium was eliminated from alloy A2 due to its extraordinary hardness and the formation of aluminium segregations, which led to Al_3Pt precipitates in alloy A1. Therefore the iron and copper contents were increased to aim for the desired hardness.

Although alloy B1 fulfils the requirements for a jewellery alloy, the alloy B2 was proposed. In this alloy gold was substituted with iron to reduce the cost of the alloy and to further simplify recyclability, since the separation of precious metals from each other is associated with higher effort and thus higher costs, as these elements can be separated only at the end of the refining process, after the non-precious elements have been separated from platinum (33). Iron behaves similarly to gold in platinum and should not change the hardness of the alloy. A small amount of yttrium was added to increase the flowability of the melt and to achieve a fine-grained microstructure.

In alloy C2 iridium was substituted by iron due to better recyclability. Palladium and iron are completely soluble in platinum and offer solid solution hardening. Manganese and tungsten were added as strong solid solution hardeners with high solubility. Germanium is a very good hardener and reduced the liquidus temperature, since the melting interval of the initial alloy C1 was too high and the alloy was too soft.

In alloy D2 copper and palladium remained as 100% soluble elements. Instead of gold, iron was used for solid solution hardening to lower the melting interval, reduce the cost of the alloy and to improve recyclability. Manganese remained as a strong solid solution hardener with high solubility. Since the initial alloy D1 was too soft and its melting interval was too high, germanium was added to D2 for improvement.

In alloy E2 manganese as a strong solid solution hardener with high solubility was slightly reduced in comparison to the initial alloy E1. Iridium and rhodium were eliminated due to difficulties in recyclability and were substituted by iron. Yttrium was added to improve flowability of the melt and to lower the melting interval.

Figure 16 shows the results of the second alloy iteration concerning the presence of precipitates. Compared to the first alloy iteration all five alloys show a sufficient solid solution microstructure.

Solidus temperature and hardness are shown in **Table V** and the changes in solidus temperatures were as follows.

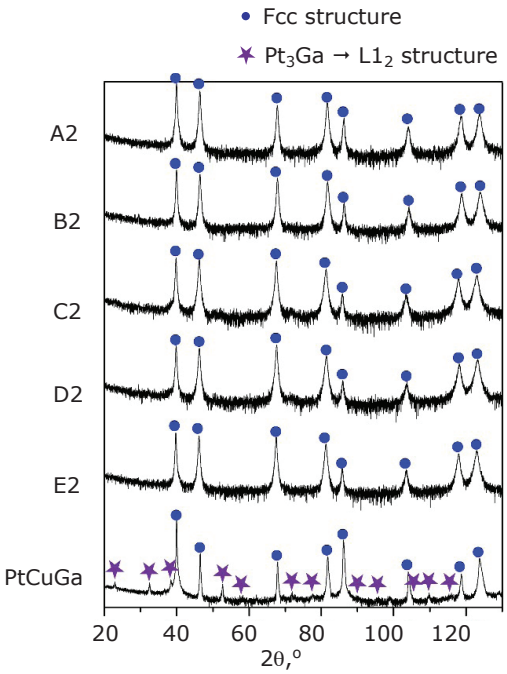

Fig. 16. XRD measurements of the five alloys of the second iteration processed by arc melting in comparison to the benchmark alloy Pt-1.8 wt% Cu-2.9 wt% Ga

Table V Solidus Temperature and Hardness of the Five Alloys of the Second Iteration Processed by Arc Melting in Comparison to the Benchmark Alloy Pt-1.8 wt% Cu-2.9 wt% Ga

Alloy	T_s in °C	Hardness[a] in HV1
PtCuGa	1320	225 ± 25
A2	1580	164 ± 12
B2	1630	165 ± 10
C2	1600	203 ± 13
D2	1410	188 ± 26
E2	1500	161 ± 11

[a] Each value was determined from an average of 20 measurements

The solidus temperature of alloy A2 was increased by 180°C compared to alloy A1, since aluminium was replaced by iron, which does not decrease the liquidus temperature by the same amount. The solidus temperature of alloy B2 was increased by 100°C compared to B1, while the solidus temperatures of C2, D2 and E2 were reduced in comparison to their counterparts in the first iteration mainly by the addition of the element germanium. The former solidus temperature ranges of C1, D1 and E1 were between 1700–1800°C while in the second iteration a reduction by up to 300°C to 1400–1600°C was achieved for all three alloys.

With regard to the hardness values the hardness range was met by A2 after strongly reducing the high hardness of the former alloy A1. B2 stayed at the same hardness level as B1 and E2 met the hardness requirements by a slight hardness increase of about 14 HV1 compared to alloy E1. D2 slightly exceeded the hardness range, while D1 was too soft. The largest increase was obtained from alloy C1 with 95 HV1 to C2 with 200 HV1. In comparison to the first iteration with only one alloy meeting the required hardness range, the three alloys A2, B2 and E2 were in the defined range of 155–170 HV1.

Therefore alloy B1 of the first iteration and all five alloys of the second iteration (A2–E2) were suitable for further investigation on microstructure and mechanical properties. These six alloys were further processed by precision casting and compared to the benchmark alloy PtCuGa.

Figure 17 shows the melting intervals determined by the casting machine pyrometer and the solidus temperatures from the pyrometer attached to the arc melting furnace. It is observed that the values for the two pyrometers correspond very well. Although all newly developed alloys had a higher liquidus temperature than the benchmark alloy PtCuGa there was enough room for overheating the melt to guarantee the complete filling of filigree parts. In addition, all melting intervals were equal to or smaller than the melting interval of PtCuGa.

3.2 Microstructure of Cast Parts

The data on porosity volume fraction and maximum pore diameter of the precision cast parts are listed in **Table VI**. Except for D2 all alloys showed very low porosity volume fractions for as-cast parts. Concerning the maximum pore diameter only B1 and B2 came close to the derived maximum pore size of 10 µm. But all alloys, except C2, showed a smaller maximum pore diameter than the benchmark alloy PtCuGa.

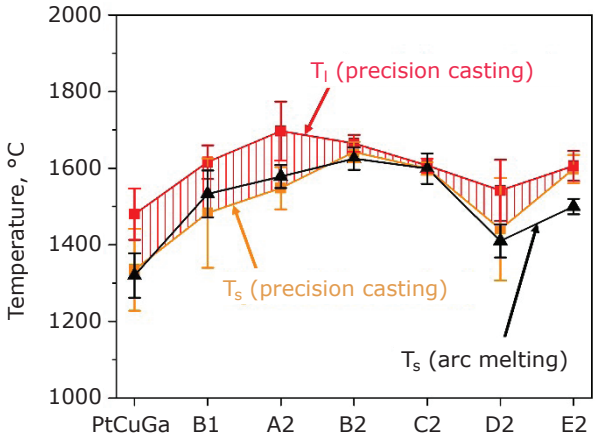

Fig. 17. Melting intervals obtained by the casting machine pyrometers (T_l and T_s) and the arc melting furnace (T_s only). Each value was determined from an average of five measurements

Table VI Porosity Volume Fraction and Maximum Pore Diameter of the Six Alloys in Comparison to Pt-1.8 wt% Cu-2.9 wt% Ga

Alloy	Porosity volume fraction in %	Maximum pore diameter in µm
PtCuGa	1.1	29
B1	0.4	12
A2	1.3	27
B2	2.9	14
C2	2.3	37
D2	5.2	27
E2	0.2	28

Figure 18 shows the results of the investigation of the average grain sizes. The requirement for the new platinum alloy was a grain size of 100–150 µm, as a fine grained microstructure promotes better mechanical properties and a high polished surface quality (19). The minimum required grain size below 150 µm was only achieved for parts with smaller diameters. For cast parts with a diameter of 20 mm the average grain sizes ranged from 1000–1800 µm. For parts with a smaller diameter of 4 mm, which would be the dimensions of a ring, the required grain size was only met by the alloy C2. For parts of diameter 2.5 mm the alloys B2, C2 and E2 were very close, while alloy D2 reached a grain size of 80 µm. For smaller diameters <1 mm the alloys C2, D2 and E2 were very fine grained, followed by B1 and B2. The results of the precision casting show that the microstructure of PtCuGa tends to be more coarse-grained than the newly developed platinum alloys.

Figure 18 shows alloy B1 with a fine grained microstructure. Even more fine grained were the microstructures of the alloys C2 and E2, which had a germanium content of 1.0 wt% and 0.3 wt%. Despite the fine grained microstructure the negative aspect was that the germanium strongly segregated at the grain boundaries together with palladium.

Figure 19 shows a grain boundary of alloy E2 in as-cast condition. In the germanium and palladium rich segregations with up to 15 wt% germanium and up to 9 wt% palladium the formation of $(Pt,Pd)_3Ge$ or $(Pt,Pd)_2Ge$ was promoted. A second

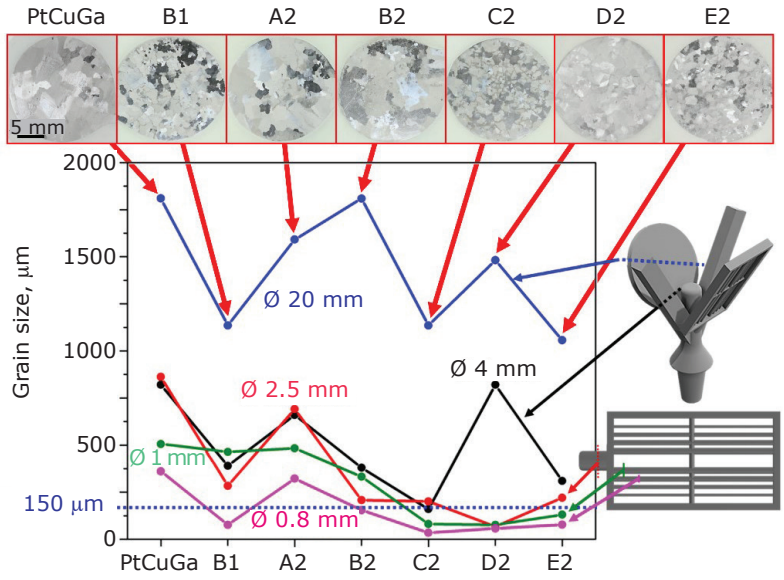

Fig. 18. Grain size depending on the local diameter of the as-cast part

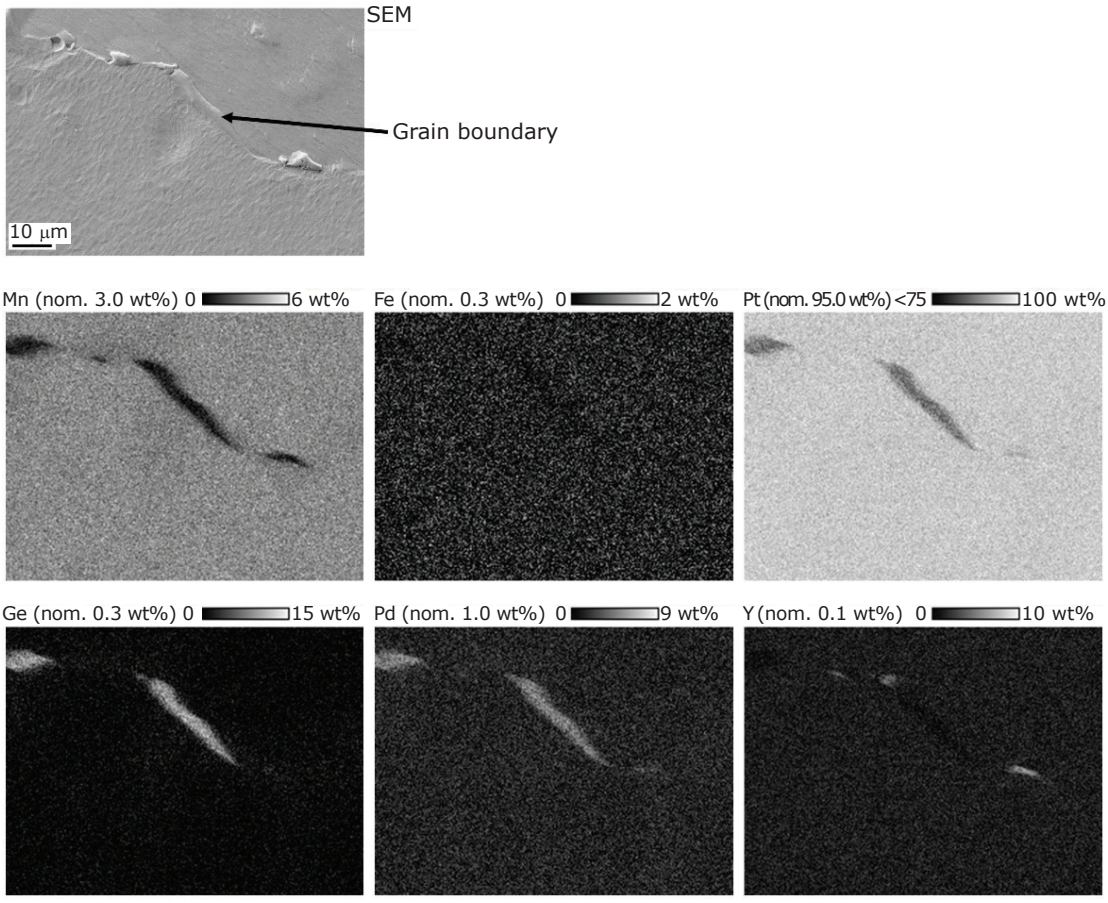

Fig. 19. Elemental distribution of germanium, palladium and yttrium in alloy E2

type of segregation was found located at the grain boundaries, consisting of a platinum, palladium and yttrium rich part with up to 9 wt% palladium and up to 10 wt% yttrium, which promotes the formation of $(Pt,Pd)_5Y$ or $(Pt,Pd)_3Y$. By the formation of these phases at the grain boundaries the brittleness was increased, leading to cracks along the grain boundaries of the as-cast samples.

Figure 20 shows microstructures of B1 and A2–D2. In alloy B1 only palladium segregations and in B2 only yttrium segregations were observed. Similar to E2, the alloys C2 and D2 also showed segregations of palladium and germanium. The benchmark alloy PtCuGa and A2 were the only ones to show no segregation and no cracks along grain boundaries.

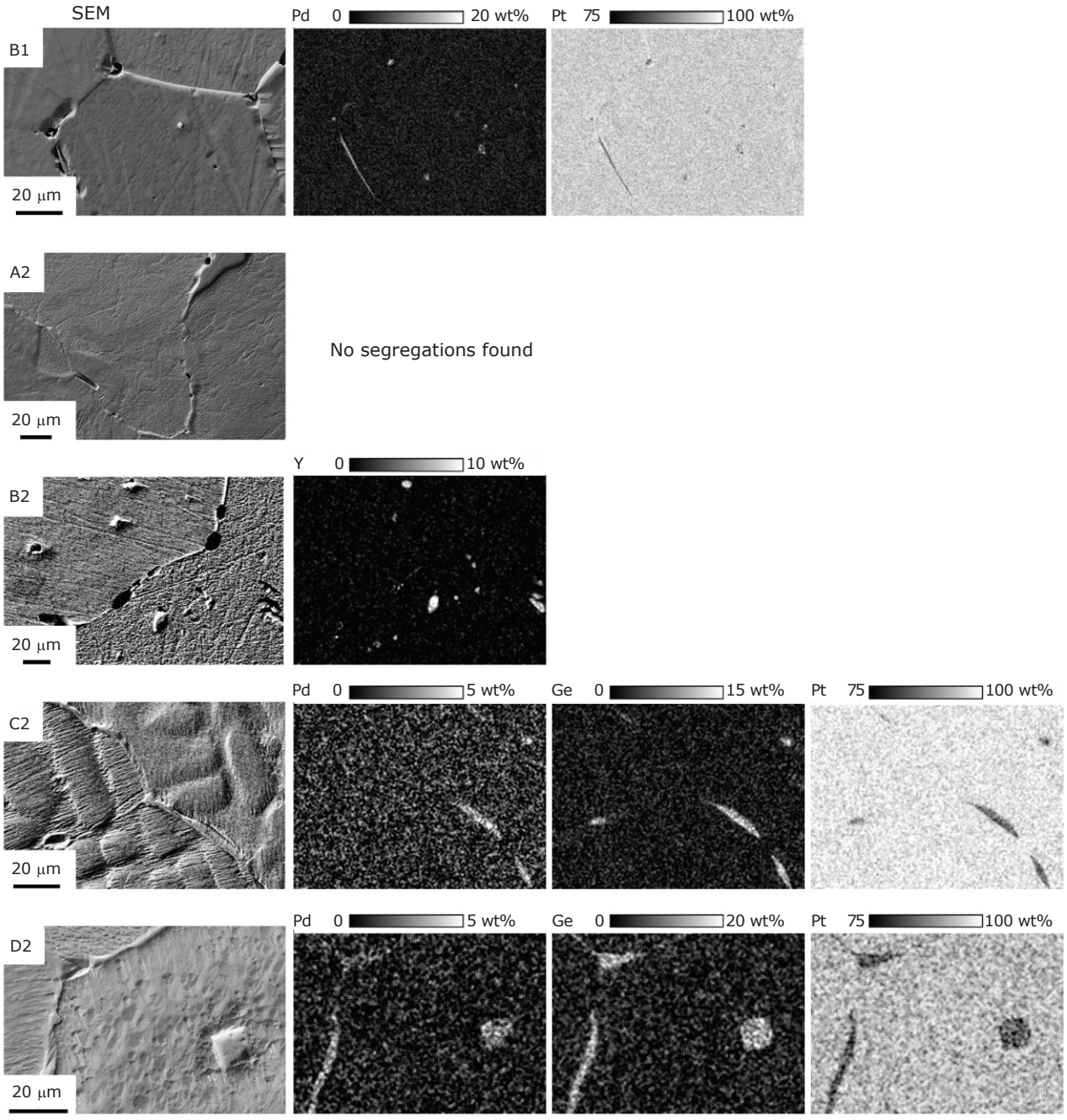

Fig. 20. Elemental distribution of yttrium, palladium, germanium and platinum in the alloys B1, A2–D2

3.3 Mechanical Properties

In addition to the arc melted samples the hardness of the cast parts was also measured, since segregations in the alloys have an influence on the hardness.

Figure 21 shows the results of the hardness measurements of the arc melted samples compared to the cast samples. It is observed that the hardness of the cast PtCuGa was lower than that of the arc melted sample, but still higher than the hardness of 165 HV1 (34) and the hardness of 173 HV1, which is due to an additional heat treatment. A higher hardness of the cast sample was measured for alloy D2, where the most segregations were detected due to the high germanium content. This was the alloy with the highest standard deviation, because of the large interdendritic areas, which show a higher hardness than the dendrite core. In summary the hardness measurements of the as-cast parts were consistent and in good agreement with the hardness measurements of the arc melted samples. The alloys A2, B2 and E2 were within the required hardness range of 155–170 HV1 in the as-cast condition.

The results of the tensile tests of the as-cast samples are shown in **Figure 22**. It is observed that PtCuGa exhibits the highest tensile stress compared to the newly developed alloys. Considering the tensile to yield strength ratio (UTS/YS), a value for strain hardening, the best value of 1.5 was obtained for Pt-1.8 wt% Cu-2.9 wt% Ga, B1 and A2, which is partly due to the homogeneous microstructure with low porosity and small pore diameters. Lower values were obtained for the alloys B2 and E2. C2 and D2, the samples with the most cracks and high porosity, failed almost immediately after reaching the yield stress. Concerning elongation to failure, which should be as high as possible to guarantee optimal machining after casting, A2 reached a similar ε_f to PtCuGa but the standard deviation was quite high for the as-cast samples. B1 achieved an elongation of about 12% and the failure of the other alloys occurred at very low elongations.

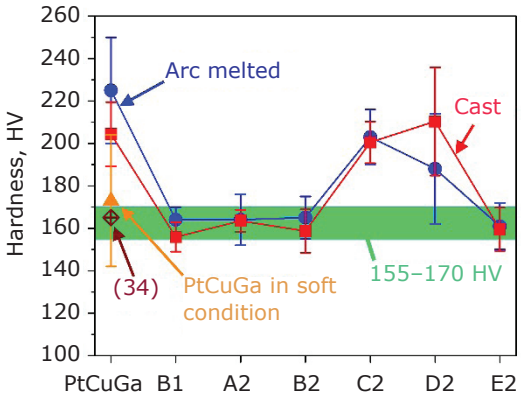

Fig. 21. Hardness (HV1) of arc melted and cast samples. Each value was determined from an average of 20 measurements. The values of PtCuGa are also given in soft condition (34)

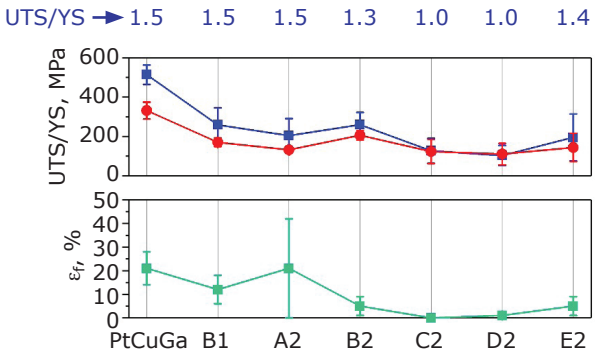

Fig. 22. Ultimate tensile strength, yield strength and elongation to failure in as-cast condition

3.4 Optical Properties

Since the alloy is intended for the manufacture of jewellery the colour and reflectivity are of great importance. The colour should be as white and bright as possible and the surface of the polished alloy highly reflecting.

Figure 23(a) shows the measured CIE coordinates L*, b* and a*. All alloys were located in the red-yellow area of the CIELab space and showed similar values of a*. They varied mainly in b* values, with C2 and E2 tending to be more yellow, while A2 and D2 had an equal b* value to that of PtCuGa. B2 was the least yellow alloy. The alloys with the least brightness were PtCuGa and C2, while B2 was the brightest of all the alloys. **Figure 23(b)** shows the values of reflectivity against wavelength in comparison to the benchmark alloy PtCuGa by measuring the difference in reflection. PtCuGa had the lowest reflectivity together with the alloy C2, whose reflectivity decreased with increasing wavelength. E2 was slightly above the line of PtCuGa with a difference of 0.5% and the alloys A2 and D2 showed higher reflectivity by about 1%. The best values were achieved for B1 and B2 with a difference of up to 5% in reflection at the shorter wavelengths. The results show that all alloys except for C2 surpassed the benchmark alloy PtCuGa in colour and reflectivity.

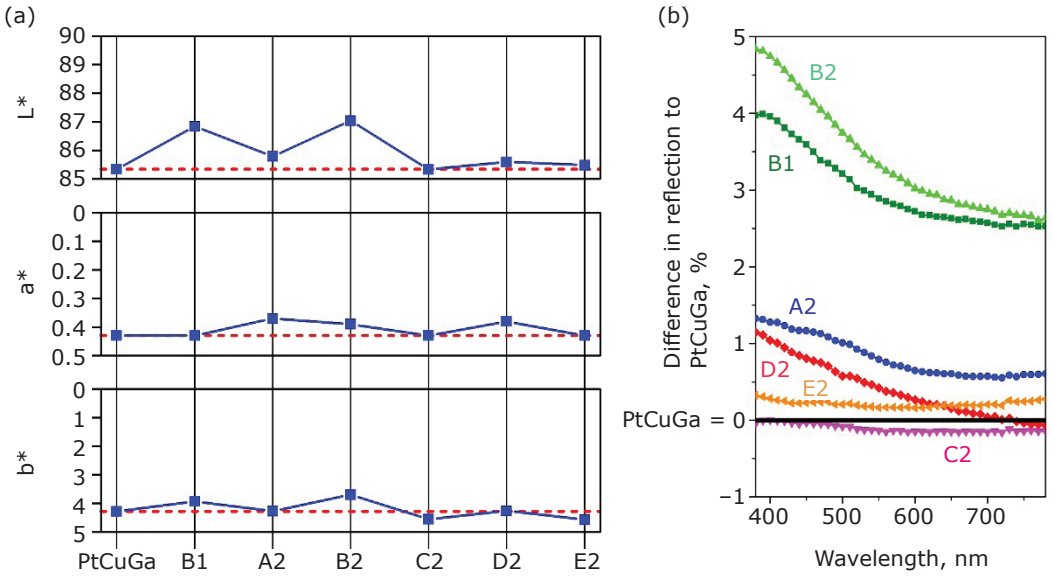

Fig. 23. (a) Colour; and (b) reflectivity of the newly developed alloys in comparison to the benchmark alloy Pt-1.8 wt% Cu-2.9 wt% Ga

4. Conclusion

Based on our definition of Equation (i) for developing a new platinum jewellery alloy, the alloy B1 (**Table II**) was obtained in the first iteration of alloy development during the present work. By recomposing the first five alloys, a second alloy iteration with another five suitable compositions was developed (A2–E2) (**Table III**). The six alloys designated B1 and A2–E2 fulfil the requirements set out in **Figure 1**.

XRD measurements revealed a single-phase solid solution for all six alloys and a smaller grain size than the currently used jewellery alloy PtCuGa. In addition the as-cast microstructures, except for alloy D2, showed a low porosity volume fraction. SEM-EDS measurements revealed intermetallic phases, rich in germanium, palladium and yttrium at the grain boundaries, causing intergranular cracks. These cracks had a negative influence on the mechanical properties of the as-cast parts and reduced the strain to failure and thereby deformability of the alloy.

Except for the alloys C2 and D2, which exceeded the upper hardness limit of 170 HV1, all other alloys developed in this work were in the desired range of 155–170 HV1, which ensures optimal wear resistance. Concerning the optical properties, all alloys except for C2 were whiter and more reflecting than PtCuGa. B2 showed the best colour and reflectivity.

The alloys A2 and B2 were therefore chosen as the two best alloy compositions considering the requirements for platinum jewellery alloys. To find the best castable alloy, different casting parameters with varying mould temperatures and overheat of the melt will be tested in the future.

References

1. "PGM Market Report May 2017: Summary of Platinum Supply and Demand in 2016", Johnson Matthey, London, UK, 2017, 53 pp
2. 'Jewellery – Fineness of Precious Metal Alloys', ISO 9202:2014, International Organization for Standardization, Geneva, Switzerland, 2014
3. J. J. Maerz, 'Casting Tree Design and Investment Technique for Induction Platinum Casting', The Santa Fe Symposium on Jewelry Manufacturing Technology, Albuquerque, USA, 19th–22nd May, 2002, pp. 335–351
4. A. Nooten-Boom II, 'Dynamics of the Restricted Feed Tree', The Santa Fe Symposium on Jewelry Manufacturing Technology, Nashville, USA, 10th–13th September, 2006, pp. 387–419
5. "Binary Alloy Phase Diagrams", 2nd Edn., eds. T. B. Massalski, H. Okamoto, P. R. Subramanian and L. Kacprzak, ASM International, Ohio, USA, 1990
6. G. Raykhtsaum, *Platinum Metals Rev.*, 2013, **57**, (3), 202
7. "Edelmetall-Taschenbuch", 2nd Edn., ed. A. G. Degussa, Hüthig-Verlag, Heidelberg, Germany, 1995
8. T. Biggs, S. S. Taylor and E. van der Lingen, *Platinum Metals Rev.*, 2005, **49**, (1), 2

9. G. Ainsley, A. A. Bourne and R. W. E. Rushforth, *Platinum Metals Rev.*, 1978, **22**, (3), 78
10. D. Miller, K. Vuso, P. Park-Ross and C. Lang, *Platinum Metals Rev.*, 2007, **51**, (1), 23
11. P. Battaini, *Platinum Metals Rev.*, 2011, **55**, (2), 74
12. T. Laag and H.-G. Schenzel, C. Hafner GmbH and Co KG, 'Platinum Alloy and Jewellery Object Produced using said Platinum Alloy', *European Patent Appl*. 2013/2,650,394
13. C. W. Corti, *Platinum Metals Rev.*, 2007, **51**, (1), 19
14. D. Miller, T. Keraan, P. Park-Ross, V. Husemeyer and C. Lang, *Platinum Metals Rev.*, 2005, **49**, (3), 110
15. S. Vorberg, M. Wenderoth, B. Fischer, U. Glatzel and R. Völkl, *J. Min. Metals Mater. Soc.*, 2004, **56**, (9), 40
16. C. H. Liebscher and U. Glatzel, *Intermetallics*, 2014, **48**, 71
17. P. J. Hill, N. Adams, T. Biggs, P. Ellis, J. Hohls, S. S. Taylor and I. M. Wolff, *Mater. Sci. Eng.: A*, 2002, **329–331**, 295
18. G. Normandeau and D. Ueno, 'Platinum Alloy Design for the Investment Casting Process', in "Platinum Manufacturing Process", Vol. 8, Platinum Day Symposium, New York, USA, March, 2000, Platinum Guild International, Newport Beach, California, USA, pp. 41–49
19. T. Murakami, R. Sahara, D. Harako, M. Akiba, T. Narushima and C. Ouchi, *Mater. Trans*., 2008, **49**, (3), 538
20. M. Wenderoth, S. Vorberg, B. Fischer, Y. Yamabe-Mitarai, H. Harada, U. Glatzel, and R. Völkl, *Mater. Sci. Eng.: A*, 2008, **483–484**, 509
21. K. Teichmann, C. H. Liebscher, R. Völkl, S. Vorberg and U. Glatzel, *Platinum Metals Rev.*, 2011, **55**, (4), 217
22. R. Völkl, M. Wenderoth, J. Preussner, S. Vorberg, B. Fischer, Y. Yamabe-Mitarai, H. Harada and U. Glatzel, *Mater. Sci. Eng.: A*, 2009, **510–511**, 328
23. Y. Rudnik, R. Völkl, S. Vorberg and U. Glatzel, *Mater. Sci. Eng.: A*, 2008, **479**, (1–2), 306
24. D. Ott, 'Problems with Investment Casting of Jewellery Alloys', Third European Precious Metals Conference, Florence, Italy, 17th–19th September, 1997
25. D. Miller, T. Keraan, P. Park-Ross, V. Husemeyer, A. Brey, I. Khan and C. Lang, *Platinum Metals Rev.*, 2005, **49**, (4), 174
26. U. E. Klotz and T. Drago, *Platinum Metals Rev.*, 2011, **55**, (1), 20
27. T. Fryé and J. Fischer-Buehner, 'Platinum Alloys in the 21st Century: A Comparative Study', Jewelry Technology Forum, Legor Group SPA, Bressanvido, Italy, 2014, 24 pp
28. 'Pro HT-Platinum: Material Safety Data Sheet', GoldStar Powders, Stoke-on-Trent, UK, 2011
29. 'Pro-HT Platinum: High Temperature Investment Powder', GoldStar Powders, Stoke-on-Trent, UK: https://www.goldstarpowders.com/products/ht-platinum (Accessed on 15th June 2018)
30. R. Völkl, B. Fischer, M. Beschliesser and U. Glatzel, *Mater. Sci. Eng.: A*, 2008, **483-484**, 587
31. R. Völkl, D. Freund and B. Fischer, *J. Test. Eval.*, 2003, **31**, (1), 35
32. "Radiometric and Photometric Characteristics of Materials and their Measurement", CIE 038-1977, Commission Internationale de l'Éclairage, Vienna, Austria, 1977, 214 pp
33. C. Hagelüken, *Chim. Oggi*, 2006, **24**, (2), 14
34. 'Materials for Jewellery and Decorative Applications', C. Hafner GmbH and Co KG, Wimsheim, Germany: https://www.c-hafner.de/en/leistungen-und-produkte/precious-metal-products/materials/materials-for-jewellery-and-decorative-applications/ (Accessed on 12th June 2018)

The Authors

Tanja Trosch has a BEng in Mechanical Engineering from the University of Applied Sciences Regensburg, Germany, and a MSc in Materials Science and Engineering from the University Bayreuth, Germany. She works as a scientific researcher and PhD student at the Chair of Metals and Alloys at the University Bayreuth, Germany. Her main interests are precious metals for jewellery application and high temperature materials.

Dr Fanny Lalire is Diploma Engineer in Material Researches (ESIREM, France) and holds a PhD in Material Sciences from CEA Valduc & Jean-Lamour Institute in France, in the field of martensitic phase transformation in nuclear alloys. She works as an R&I Project Manager in the Material Innovation Department of VARINOR SA in Delémont, Switzerland. Her main skills are directly linked with precious metal development and material properties calculations.

Dr Stephane Pommier was awarded a Master's degree in Physics and Chemistry of High Performance Materials in 2010 and a PhD in Materials Science in 2014 by the University of Limoges, France. His doctoral study was achieved in close collaboration with ERAMET group, France. At present, Dr Stephane Pommier works as an R&I project manager for VARINOR SA in Delémont, Switzerland, where he is the head of the alloy development laboratory.

Dr-Ing Rainer Völkl is academic councillor and senior researcher at the Chair of Metals and Alloys at the University Bayreuth, Germany. His main fields of research include alloys of the platinum group metals as well as nickel-base alloys, testing of mechanical properties at high temperatures and electron microscopy.

Professor Dr-Ing Uwe Glatzel is head of the Chair of Metals and Alloys at the University Bayreuth, Germany. His work had a big impact on the development of modern high temperature alloys, mainly nickel-based superalloys. He advises several research groups on developing new alloys for high temperature applications, laser metallurgy, material analysis and artificial knee joints.